Arch. Metall. Mater. **71** (2026), 1, 375-386

DOI: https://doi.org/10.24425/amm.2026.157800

P. SURULIMANI[1*], B. RADHA KRISHNAN[1]

MICROSTRUCTURAL AND MECHANICAL EVOLUTION OF AA6063/WC COMPOSITES UNDER AGING AND ROLLING CONDITIONS

This study aims to refine a rheo-stir casting method for producing aluminium alloy 6063-based metal matrix composite reinforced with tungsten carbide at varying concentrations ranging from 0.2% to 1% by weight. AA6063/0.6WC composite was subjected to additional testing, and this shows how operations, including solution heat treatment and rolling under different circumstances, impacted the material. A closer look at the microstructure reveals that the pining effect caused by the integration of WC into the AA6063 matrix resulted in grain refinement. As the amount of increasing WC addition, the material's mechanical characteristics enhanced. The composite with 1 wt.% WC exhibited the maximum microhardness (98 Hv), Ultimate tensile strength (UTS) (235 MPa) and Yield strength (YS) (210 MPa) due to the dispersion strengthening mechanism. The densification and particle dispersion of AA6063/WC composites were greatly improved by the rheo stir casting method. Hardness was improved by precipitation hardening after the secondary phases were dissolved in a homogenization procedure. Because dynamic recovery was inhibited during cryo- rolling, the resulting specimen had the maximum hardness of 178 Hv among all rolling techniques while being 80% thinner. It was shown that experimental YS was greater than theoretical YS after accounting for the impact of the strengthening processes.

Keywords: AA6063/WC; Aging; Rolling; mechanical properties; Optical Microscope; Stir casting

1. Introduction

The aerospace and automobile sectors both make extensive use of aluminium alloys (AA) because of their numerous useful qualities. AA6063/WC composites are recommended for aerospace, automotive, tool, and marine applications due to their enhanced hardness, tensile strength, and wear resistance. Their advantageous mechanical properties are appropriate for applications where components are stressed, and/or under wear and corrosion including engine parts, brake components, structural parts and buildings, cutting tools, and armor. They have a low density, are quite rigid for their weight, and are very light [5]. The need for stronger yet lighter materials to improve performance meant that aluminium alloys were rarely used in structural engineering [6].

This led to the development of aluminium-based composites with a variety of reinforcing materials [22]. One of the reasons why manufacturers use monolithic materials and aluminium alloys is that they can be easily modified to provide the specific mechanical qualities needed for AMMCs [4]. TiC, SiC, Al_2O_3, B_4C, TiB_2, and ZrB_2 ceramic particles are widely considered for usage as possible reinforcements in the development of AMMCs. According to the results of the experiments, the composite can achieve the necessary qualities by using reinforcement that is well-chosen for the matrix alloy [21,22]. The production technique, the shape, size, and ratio of ceramic particles, as well as other ideal characteristics, may all contribute to the desired features. Micron-sized ceramic particles have been shown in experiments to strengthen the produced composite but also reduce its ductility, restricting its use to only a few niche applications [20]. Titanium carbide (TiC) has micron-size particles that are extremely strong, have increased ductility, are excellent raised-temperature materials, and have exceptional wear resistance [16]. TiC is preferable to other reinforcements because of its improved mechanical qualities.

The manufacturing method is crucial to the evolution of composites since it affects the ultimate properties of the materials. There are primarily three types of fabrication methods: those that take place in a solid state, those that take place in a liquid state, and those that take place in situ [27]. Liquid metallurgy processes that might be used to manufacture a wide range of large-scale composites. Due to its ease of use, adaptability, cheap cost, and commercial viability, stir casting has emerged

[1] DEPARTMENT OF MECHANICAL ENGINEERING, NADAR SARASWATHI COLLEGE OF ENGINEERING AND TECHNOLOGY, THENI, TAMILNADU, INDIA

* Corresponding author: surulimani@nscet.org

as the method of choice for producing aluminium matrix composites [7]. Particle segregation on grain boundaries and matrix porosity are still problems with stir-casting AMMCs, despite using optimal restrictions [26].

These treatments have the potential to drastically cut down on porosity, even out the distribution, alter the development of secondary phases, and change the microstructure [12,23]. Micro-segregation and residual components at grain boundaries are common in castings of the AA7XXX series due to the high quantity of alloying elements found in these alloys, which can have a negative impact on mechanical qualities [1,2].

The precipitation hardening behavior that results in hardness, tensile, and flexural strengths increasing with varying ageing time is observed in the B_4C-reinforced Al7075 composites up to an optimal aging time. The hard B_4C particles increase ageing rate leading to more uniform microstructure with less porosity. However, over-ageing diminishes these good properties which underlines that the ageing period should be optimised for the best combination of strength and wear resistance [9].

The squeeze casting performance of B_4C-whisker to AA7075 composite has been studied. B_4C agglomerates in particles at high concentrations, however adding 4-12 wt.% increases the tensile strength, bending strength, hardness, wear resistance and elastic modulus. The matrix of reinforced composites is harder and more wear-resistant than nonreinforced alloy, as demonstrated by optical spectroscopy, scanning electron spectroscopy, and energy dispersion spectroscopy. B_4C particles enhance the mechanical and tribological characteristics of AA7075, demonstrating that ceramic dispersion may effectively strengthen aluminium alloy [28].

A new Al7075/TiO_2/kaoline hybrid composite is prepared by Technique of high-energy ball milling and subsequent sintering. The addition of kaoline as well as the increase of sintering temperature were beneficial to rise microhardness and decrease friction coefficient. The wear rate decreased significantly for larger kaoline reinforcement, with only plastic deformation detected after testing. Thermal analysis indicated endothermic and exothermic reactions at temperatures between 635°C and 750°C; no unwanted phases were present [32].

During an efficient homogenization process, the dendritic structure is altered, any residual coarse particles are broken down, and the solute is evenly distributed throughout the matrix [14]. Cryo-rolling is a deformation process that uses liquid nitrogen to create ultrafine grain (UFG) structures with numerous dislocation tangles [8]. Cryogenic deformation produces UFG microstructures that are superior to more traditional ways of supplying mechanical characteristics in Al alloys and FCC metals [25].

However, it came as a surprise to hear that no research has been done on the importance of WC in AMMCs. This work examined how WC inclusion affects the microstructure and mechanical properties of rheo stir cast AA6063 composites. The goal of this study was to determine how modifying both the microstructure and the mechanical characteristics of manufactured composites through solutioning and rolling could improve their mechanical qualities.

2. Material and methods

In this work, plates made of AA6063 were utilised as the matrix, the TABLE 1 shows the chemical composition of AA6063, which was used as matrix material.

TABLE 1

Chemical composition of AA6063 alloy (wt.%)

Element	Zn	Cu	Mg	Si	Cr	Fe	Mn	Al
Weight %	0.10	0.10	0.90	0.60	0.10	0.35	0.10	Balance

The WC particles have a granule size of 5 μm. Fig. 1(a) and Fig. 1(b) present the SEM images of the received AA6063 and WC powder, respectively.

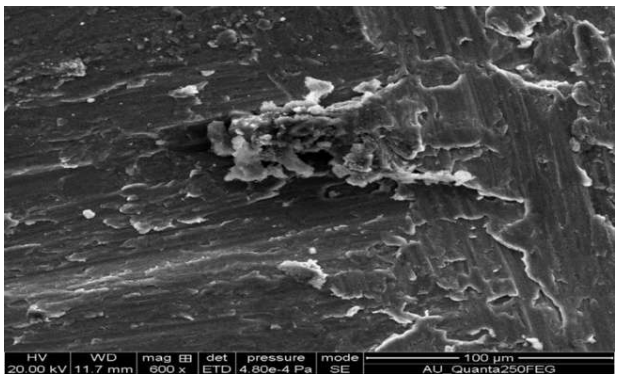

Fig. 1(a). SEM image of AA6063

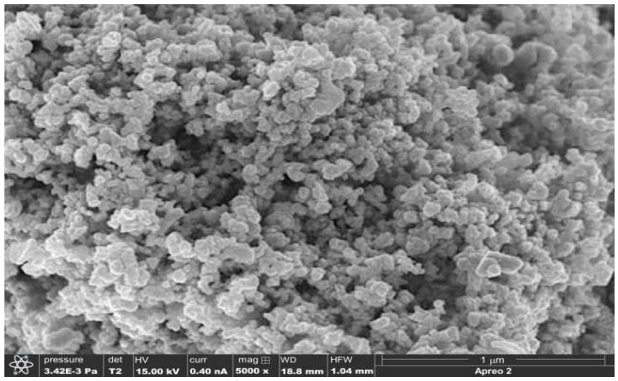

Fig. 1(b). SEM image of as-received WC Powder

Rheo stir casting was used to create the AA6063-WC composites, the casting setup showed in Fig. 2(a). Two-stage processing, rheo stir casting entails heating an aluminium matrix to its melting point of 660°C and subsequently reducing it gradually to its semi-solid stage temperature of 600°C. The moisture and volatile compounds were removed from the WC particles by heating them to 400°C for an hour before injecting them into a semi-solid slurry and swirling them at a rate of 50 rpm for five minutes. Dispersing the WC in the aluminium melt required the use of a mechanical stirring system, which consisted of a graphite rod and a graphite impeller with three blades. After being heated to 950°C, the composite slurry was agitated at 300 rpm for

10 minutes to restore it to the processing temperature. To get rid of the gases produced during processing, a C_2C_{l6} degassing tablet was dissolved in the slurry. The liquid was then poured using the bottom pouring technique into a 200×30×15 mm steel die that had been heated to 150°C. After the composite had formed in the die, it was quickly quenched with water.

The sample F composite (AA6063/1% WC) has the highest hardness and tensile strength compared to the other sample A to sample F composites. Therefore, using post-processing techniques, the relationship between the sample F composite's microstructure and its mechanical properties (Heat treatment and Rolling) was investigated.

The composite was used to create six identical specimens with the same volume (1000×1000×1000 mm^3). After 2 hours of rest between solutionizations, were subjected to 470°C in the muffle furnace for 2 hours up to 20 hours. The specimens were subjected to solution heat treatment, quenched in cool water, and subsequently aged at 120°C for 24 hours. Additional processes, such as rolling, were applied to the samples. Rolling specimens were 12 mm in thickness throughout the board. The rolling process is depicted schematically in Fig. 2 under a variety of operating conditions.

Fig. 2(a). Rheo stir casting setup

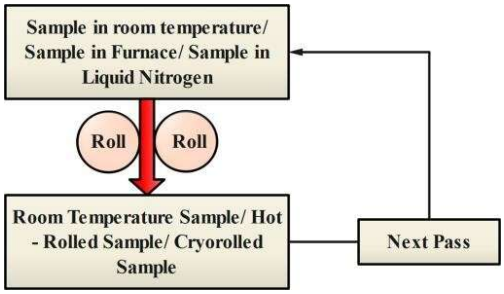

Fig. 2(b). An outline of the process of rolling

Sample F was initially subjected to hot rolling (HR), room temperature rolling (RTR), and cryo-rolling (CR). Before being put through hot rolling, samples were heated in a muffle furnace for 30 minutes at 400°C. After each CR run, the samples were submerged in liquid N_2 for 10 minutes. In order to reduce the thickness by 50% and 80%, respectively, each sample was rolled at different speeds and temperatures. High-energy rolling was accomplished using a machine with 110 mm diameter rollers that rotated at a steady 8rpm. To achieve the same thickness with fewer roller passes, we simply kept the rolling thickness reduction at 4% for every pass. Microstructure analyses of solution-treated composites, rolled composites, and as-cast composites were conducted with a LEICA DMI 5000M optical microscopy instrument and a FESEM. Using the IMAGE J application, we were able to estimate the usual grain size. First, the samples were polished to a mirror finish using emery paper of several grits and fine cloth dusted with MgO powder in preparation for microstructural characterization. Hardness testing required machining and conditioning of the samples to the specifications of ASTM standard E-92. A Vickers hardness tester was used to establish the material's hardness. The difference of ten measurements was obtained after indentations of 200 g with a dwell period of 10 s were produced at random spots on the polished surface. The tensile testing of sub-size standard samples (12.5 mm in gauge length) that met the ASTM E-8 standard was conducted on a universal testing machine.

3. Results and discussions

3.1. Mechanical properties

The mechanical characteristics of AA6063 and the resulting composite AA6063/WC were compared through tests of microhardness and tensile strength (0.2 wt.% to 1 wt.%).

3.1.1. Hardness (Vickers Micro hardness)

Fig. 3 shows the variation in hardness as a function of the percentage of WC added to the final composites by weight. The toughness of the composites has been greatly improved by the use of WC. Fig. 3 shows that the weight percent of WC and composite hardness was raised. Additionally, the produced composite has a greater hardness than as- cast AA6063 regardless of the weight percent of WC added.

Composites can be made harder through a variety of strengthening methods when brittle reinforcement is introduced into a ductile matrix [15,24]. The enhanced toughness is a result of the inherent hardness of WC and the reduction in grain size.

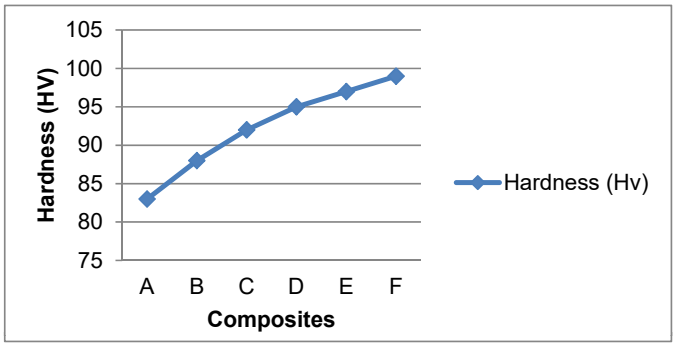

Fig. 3. Evaluation of Hardness with various composites

According to the Hall-Petch equation, hardness rises as grain size decreases. When hard WC particles are present, they restrict dislocation movement and promote strengthening, making the material more resistant to plastic deformation.

3.1.2. Tensile characteristics

The tensile test specimens are displayed in Fig. 4(a), and the stress-strain curves in Fig. 4(b) demonstrate how the tensile properties of the generated composites alter as the weight percentage of WC increases. Fig. 4 (b) illustrates how the inclusion of WC greatly improved the composites' UTS and YS. As the WC wt. Percent increases, tensile strength also increased. UTS, YS, and % Elongation were all maximized in the composite sample reinforced with 1% WC (235 MPa, 210 MPa, and 2.7%, respectively).

There is an increase in strength due to dislocation gliding on slip planes caused by the WC particles' uneven and disorganized shape. The enhanced strength of WC was investigated from a variety of angles, including the role of dispersion, thermal disparity, micromechanics, load transmission mechanism, and grain improvement [2]. TABLE 2 contains a list of the mechanical properties of AA6063 that have been reinforced with varying percentages of WC.

3.1.3. Strengthening mechanism

The addition of WC particles to AA6063 led to many different strengthening processes, which are investigated here. Mechanisms of load transmission (σ_{yc}) and micromechanics (σ_{ym}) are considered for YS's analysis. Continuum mechanics theory looks at the impact of shifting load from a soft matrix to a hard reinforcement, and Eqs. (1) and (2) described below can be used as approximations for the YS.

$$[\sigma_{ye} = \sigma_{ym} V_f \left(\frac{S+2}{2}\right) + V_m \tag{1}$$

whereas

S – Reinforcement particle aspect ratio, $S = 1$ for particles that are equiaxed

V_f – Percentage volume of reinforced particles

V_m – Percentage volume of matrix

σ_{ym} – Matrix.

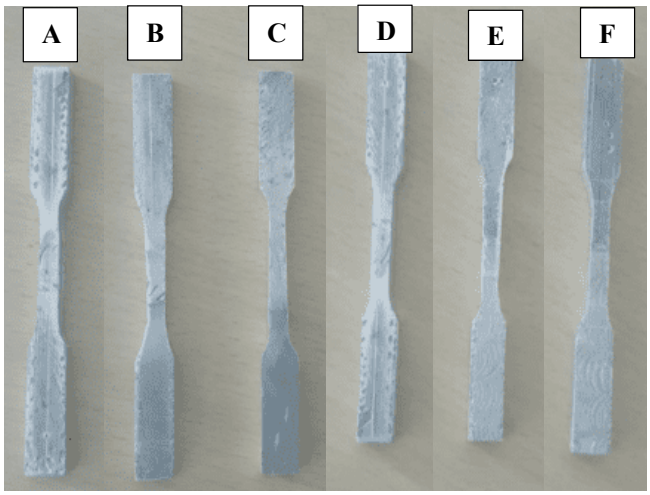

Fig. 4(a). Tensile test specimens

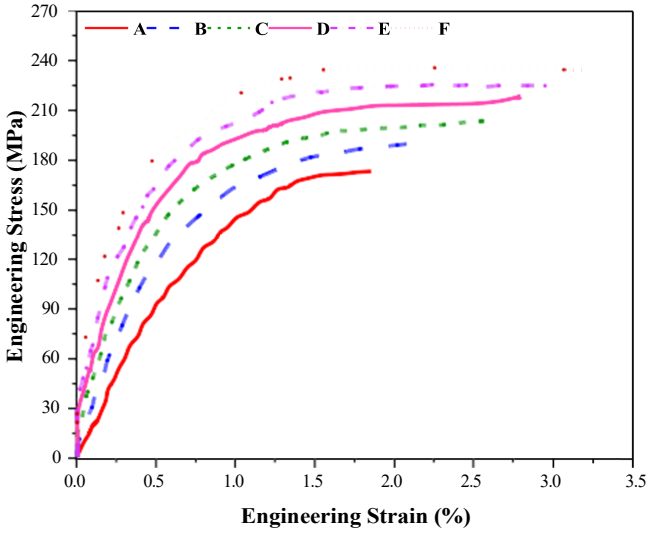

Fig. 4(b). Engineering stress-strain curvature of the various composites

$$\sigma_{ye} = \sigma_0 + \Delta\sigma_{grain-refinement} + \\ + \left[\left(\Delta\sigma_{Orowan}\right)^2 + \left(\Delta\sigma_{CTE}\right)^2\right]^{1/2} \tag{2}$$

where σ_0 is the as-cast AA6063 yield strength.

Since the particles of the reinforcements utilized in this study are 5 μm in size, the Orowan strengthening method is not applicable.

TABLE 2

Mechanical characteristics of AA6063-WC composites

S. No.	Composition	Composition code	Hardness (Hv)	Yield Strength (MPa)	Ultimate Tensile Strength (Mpa)	Percentage of Elongation	Avg. Grain (μm)
1	AA6063	A	83	108±9	152±17	1.4±0.4	138
2	AA6063+0.2%WC	B	88	125±13	167± 21	1.8±0.3	106
3	AA6063+0.4%WC	C	92	140±10	181± 15	2.1± 0.5	85
4	AA6063+0.6%WC	D	95	162.5±13	194± 18	2.4±0.4	68
5	AA6063+0.8%WC	E	97	164±11	201± 24	2.6±0.6	59
6	AA6063+1%WC	F	99	172±16	206± 28	2.8±0.7	52

TABLE 3

Evaluation of porosity and density

No	Composition	Sample Code	Theoretical density (kg/m^3)	Experimental density (kg/m^3)	Relative Density	%Porosity
1	AA6063	A	2.92	2.86	99.3	1.8
2	AA6063/0.2WC	B	2.924	2.852	98.8	2.2
3	AA6063/0.4WC	C	2.925	2.843	98.6	2.7
4	AA6063/0.6WC	D	2.936	2.834	98.2	3.1
5	AA6063/0.8WC	E	2.945	2.823	97.7	3.6
6	AA6063/1WC	F	2.952	2.810	97.2	4.1

3.2. Density

The theoretical density of the composites was derived using the law of mixtures, while the actual density was determined using the Archimedes principle. The relative density values of sample A through Sample F of the AA6063/0.2-1 wt.% WC-produced composites are presented in TABLE 3.

TABLE 3 shows that when the amount of WC increases, both the relative density and the percentage of porosity of the composite samples decrease. The up to 4% porosity increases seen in MMC stir casting are acceptable due to accumulation and porous nucleation at the boundary [3].

3.3. Evaluation of microstructure

A field emission scanning electron microscope image of a composite material reinforced with 0-1% WC reveals the presence of aluminium and grain boundary eutectic phases. Mg, Zn, Cu, and Fe solutes interact at grain boundaries to form intermetallic compounds and eutectic phases. The dendritic structure degrades and transforms into equiaxed grains, and then grain size decreases as the WC content rises (Fig. 5(b)-(c)), (f). This improvement in grain processing can be attributed to acting as pins; WC particles prevent α-Al melt granules from becoming larger. The nucleation rate is proportional to the weight

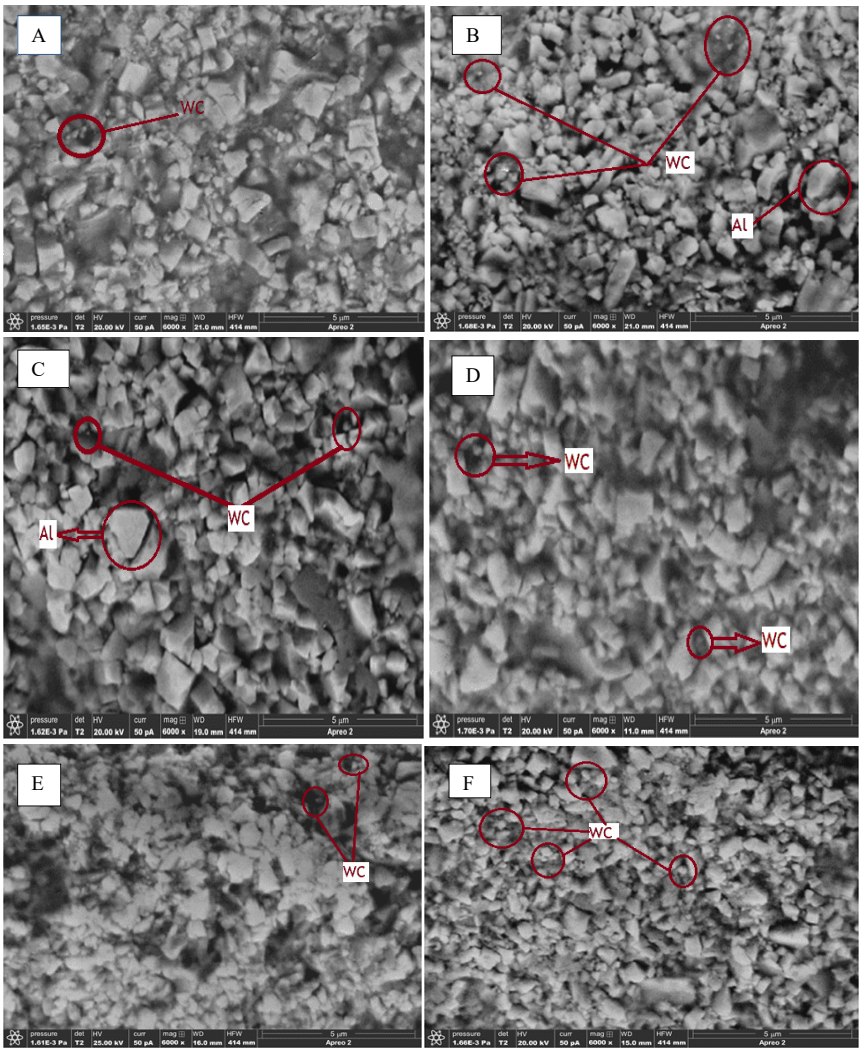

Fig. 5. FESEM images of composite with (a) 0% WC, (b) 0.2% WC, (c) 0.4 %WC, (d) 0.6% WC, (e) 0.8%WC, (f) 1% WC

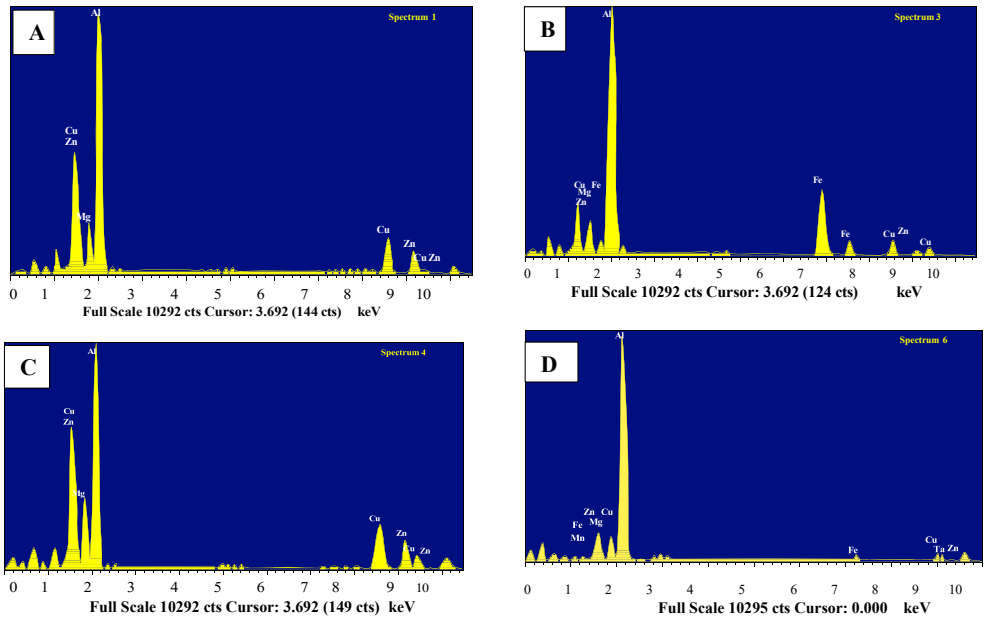

Fig. 6. (a) EDX of AA6063 with 0.2%WC (b) EDX of AA6063 with 0.4%WC, (c) EDX of AA6063 with 0.6%WC and (d) EDX profiles of AA6063 with 1% WC

percent of WC particles because these particles serve as nucleating sites.

The EDX results in Fig. 6(d) show that the WC particles are indeed separated in the inter-dendritic region. The uniformity of the WC particle dispersion is compromised by this sorting [10]. Particles' buoyant motion and the solidification pushing can both be responsible for the dispersion of WC particles during the solidification process [13]. Particles travel at different velocities along the solidification front, resulting in intergranular and intragranular dispersion. If the solidification front is moving slower than the critical velocity, the particles are pushed along with it into the intergranular zone, and the opposite is true if the front is moving faster than the critical velocity [30]. The present study demonstrates by EDX analysis that the incorporation of 5-micron particles and a substantial temperature gradient lead to a critical velocity in the intergranular zone that exceeds the solidification velocity. Specimen porosity manifests in a variety of ways throughout their exteriors. Fig. 5(b) illustrates that the incorporation of WC resulted in a significant transformation of the coarse columnar α-Al grains and certain dendritic structures into refined equiaxed grains. Increases in WC content in the grain led to a more refined product. The average particle size of AA6063 decreases to 49 μm after being refined, with some micro-voids and 1 wt.% WC, from the 135 μm observed in the as-cast material, as illustrated in Fig. 5(f).

3.4. Dislocation strengthening

At 950°C, the thermodynamic equilibrium between the reinforcing particles and matrix melt was reached. The thermal mismatch between WC and AA6063 causes thermal stresses to emerge during the solidification of the composite slurry when it cools to room temperature. The temperature differential between the tungsten carbide particles and the AA6063 matrix causes strain at their contact. The improvement in YS may be traced back to the volumetric strain caused by the CTE difference between WC and AA6063, which in turn causes the formation of geometrically required dislocations (GND) [11]. Using the following Eqs. (3) and (4), the dislocation strengthening of AA6063/1 wt.% WC was calculated [31].

$$\Delta\sigma_{CTE} = \eta G b\sqrt{\rho} \tag{3}$$

where

G – shear modulus of matrix alloy (G = 26.2 GPa),
b – burgers vector (b = 0.286 nm),
η – constant,
ρ – dislocation density determined by Eq. (4) [18].

$$\rho = \frac{12\Delta\alpha\Delta T V_f}{bDV_m} \tag{4}$$

where

D – average diameter of the reinforced particle,
DT – difference between the processing temperature and the preheated die temperature,
$\Delta\alpha$ – difference among the thermal expansion coefficients of AA6063 (23.1×106/k) WC particles (6.96×106).

The eutectic phase of Magnesium (Zinc, Copper, Aluminium) also resists dislocation motion, which contributes to the material's increased strength.

3.5. Effect of heat treatment

The microscopic separation of alloying elements in the inter-dendritic areas of the AA6063/WC composites formed

may suggest non-equilibrium solidification. It was observed that a wide variety of intermetallic phases, including Mg(Zn, Cu, Al)$_2$, (Al_2Cu), Al_7Cu_2Fe, etc., form in as-cast and developed AA6063/WC composites [29]. The produced composites need to have their secondary phases and coarse residual components dissolved using a suitable solution treatment. Solutes are now uniformly distributed over the α-Al matrix after this treatment, eliminating segregation at grain borders. In order to attain the desired composite properties, the microstructure must be changed, and the diffusion must take place over a long enough time in the solution treatment. Researchers suggest looking into how the secondary phases and residual components of AA7xxx dissolve at temperatures lower than 465°C. Authors [17] found that the rate of solute diffusion inside a matrix grew as the time of diffusion lengthened with no changes in temperature. It has been shown by authors that prolonged exposure to a constant temperature increases the likelihood that secondary phases would dissolve in the aluminium matrix. Fig. 7 shows a FESEM micrograph of a solutionised and quenched specimen (AA6063/ WC) specimen that has been aged at 120°C for 24 hours.

As can be seen in Fig. 7, solution heat-treated at 470°C for two-hour intervals dissolved the secondary phases, and age-related precipitation initiated within the grain. Fine precipitates of $MgZn_2$ and Al_2CuMg are evenly distributed inside the matrix as the ageing duration increases, as illustrated in Fig. 7. These minute precipitates play a key role in raising the hardness by impeding the motion of dislocations. The $MgZn_2$ precipitates have begun to disintegrate, as seen in Fig. 7, while the Al_2CuMg precipitates have grown coarser and are now essentially gone. Age-related formation of the black Mg_2Si phase in the α-Al matrix is verified by XRD investigation (Fig. 8). After 24 hours of ageing, only the iron-rich grey phase (Al_7Cu_2Fe) and the black Mg_2Si phase remain. These phases do not dissolve, reducing the composite's overall strength. Owing to its maximum melting point, the grey colour phase (Al_7Cu_2Fe) remains unaltered, whereas the black colour phase (Mg_2Si) changes form from linear to rounded and elliptical as ageing time increases (Fig. 7).

3.5.1. Phase analysis of aged sample F composites

The XRD results for the composite sample F that was aged at 120°C for 1 day are displayed in Fig. 8. Weak peaks for Al and WC may be seen in the XRD patterns. All the specimens,

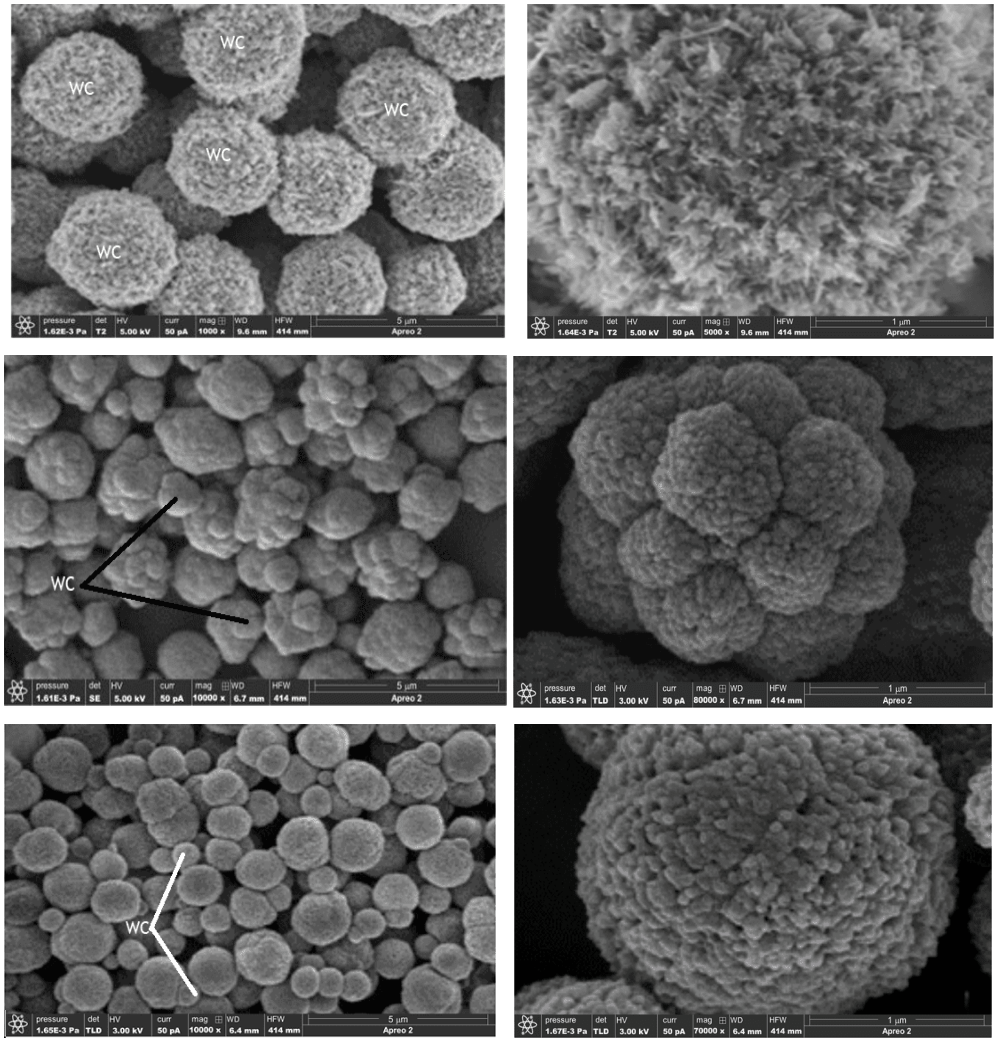

Fig. 7. FESEM image of aged samples of A-F for 24 h

regardless of how long they were aged, showed the presence of strong Al peaks and WC peaks. After 12 hours of age, the sample F have low-intensity peaks of $MgZn_2$, Al_2Cu, and Al_2CuMg began to fade. Over time, both the Al_7Cu_2Fe and Mg_2Si phases will remain insoluble.

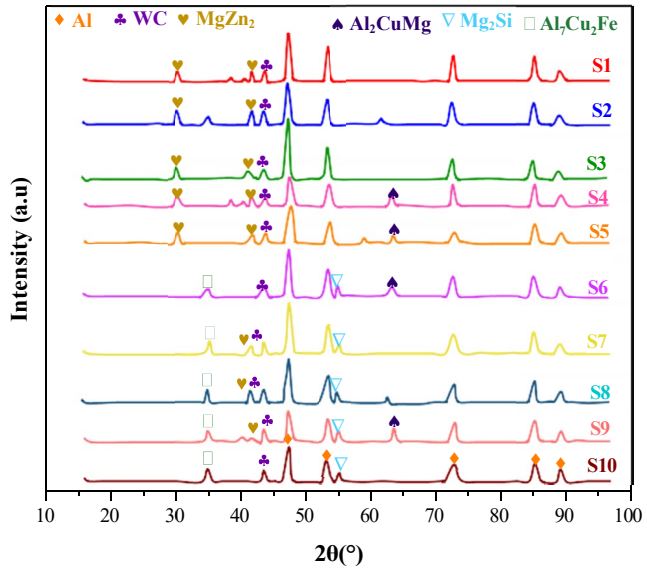

Fig. 8. XRD of aging of Sample F for 1 day

3.5.2. Hardness of aged composites

Fig. 9 displays the effect of raising the ageing temperature from 122°C to 470°C for 24 hours on the hardness of a sample solution of composite F.

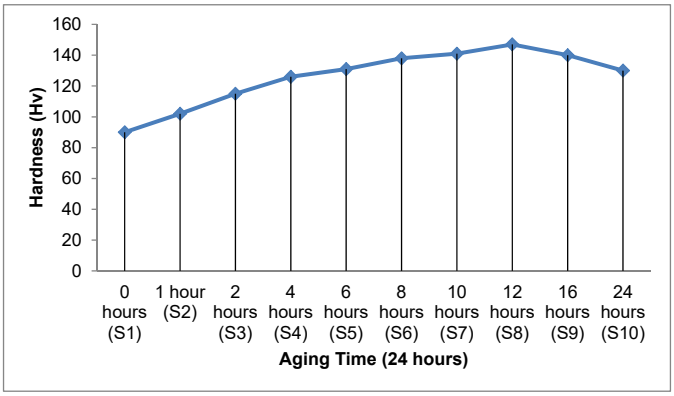

Fig. 9. Evaluation of Hardness in composite sample F with respect to ageing time

Fig. 9 shows that the sample F hardness increases steadily with ageing time up to a certain point and then gradually decreases. Hardness testing revealed that sample F may reach a maximum of 145 Hv. The lattice deformation that prevents dislocations from migrating is driven by the expansions of the saturated solid solution at solution temperatures of 470°C for as long as 12 hours. Over time, more of the matrix's dissolved components will begin to crystallize. The increase in hardness of F is due to an increase in fine precipitates, which tend to get larger and decrease in number with age. After 12 hours, the supersaturated solid solution is diminished, and the hardness is lessened because the Mg_2Si phase and the Al_7Cu_2Fe phase remain insoluble and act as an impediment to the termination of solute elements inside the matrix.

3.6. Effect of rolling

Additional research was conducted on specimen F to examine the impact of rolling under various conditions on the enhancement of hardness. The ensuing optical microstructures of specimen F after being rolled to reduce its thickness by 50% and 80% are shown in Fig. 10. During OM examination of 50% and 80% room temperature rolled (RTRed) specimens, the non-recrystallized elongated grain structures exhibited in Figs. 10(a) and 10(b) were observed (b). This might be due to the enhanced thermal cross-slip and the reduced restriction of dynamic recovery. The density of dislocations did not increase as a result of the strain energy that was generated at ambient temperature. An 80% rolled specimen has an average grain length of 350 µm, which is substantially longer than the average grain length of a 50% rolled specimen, which is approximately 125 µm. Figs. 10(a) and 10(b) illustrate the initial elongation of particles in the rolling direction under heightened strain, resulting in a ribbon-like configuration, followed by the fragmentation of these grains into smaller particles. The white arrows depicting the grains and sub-grains generated under different rolling conditions are consistent throughout all OM images. Figs. 10(c) and 10(d) are OM pictures of a specimen F that has been Hot rolled (HRed) at 400°C, showing a 50% and 80% thickness decrease, respectively. OM analysis shows that recrystallized grains with nuclei located along the grain, as indicated in Figs. 10(c) and 10(d). A dynamically recrystallized grain with an increased quantity of recrystallisation at the grain boundaries has been created for use in hot deformation.

Discontinuous dynamic recrystallisation (DDRX) was characterized by the simultaneous nucleation and development of recrystallized grains via a bulging recrystallisation mechanism. Figs. 10(c) and 10(d) show that the DDRX involves nucleation, grain formation, and refinement of grains. Accumulation of dislocation occurs when its destruction rate is lower than its generation rate. Nucleation happens by the bulging of preexisting grain boundaries once a certain dislocation density is reached. The formation of layers of ultrafine grains at the grain boundaries enhances toughness without a corresponding reduction in strength. For a reduction of 50%, the resulting fine grains are around 15-20 µm along the grain borders, while for a reduction of 80%, the resulting fine grains are about 10-15 µm in size. Cryo-rolled specimen F in Figs. 10(e) and 10(f) reveal optical microstructures after the decrease in thickness by 50% and 80%, respectively. Some equiaxed grains with diameters of 15 µm for a 50% reduction and 9 µm for an 80% decrease along the elongated grains may be found in the CRed samples.

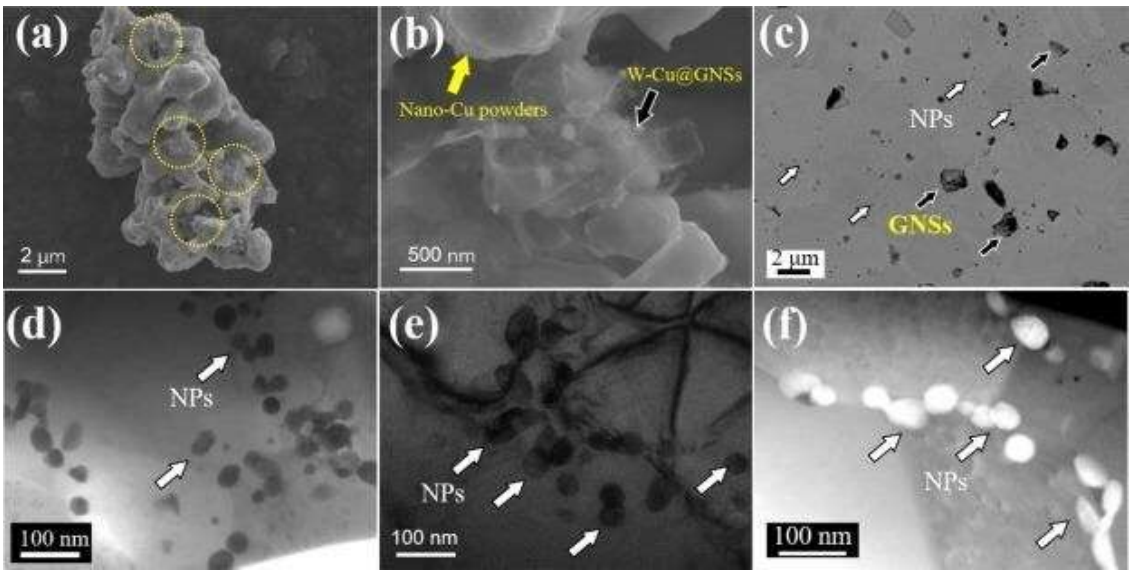

Fig. 10. Optical image of Rolling on variant situations RTR at (a) 50% (b) 80%; HR (c) at 50% (d) 80%; CR at (e) 50% (f) 80%

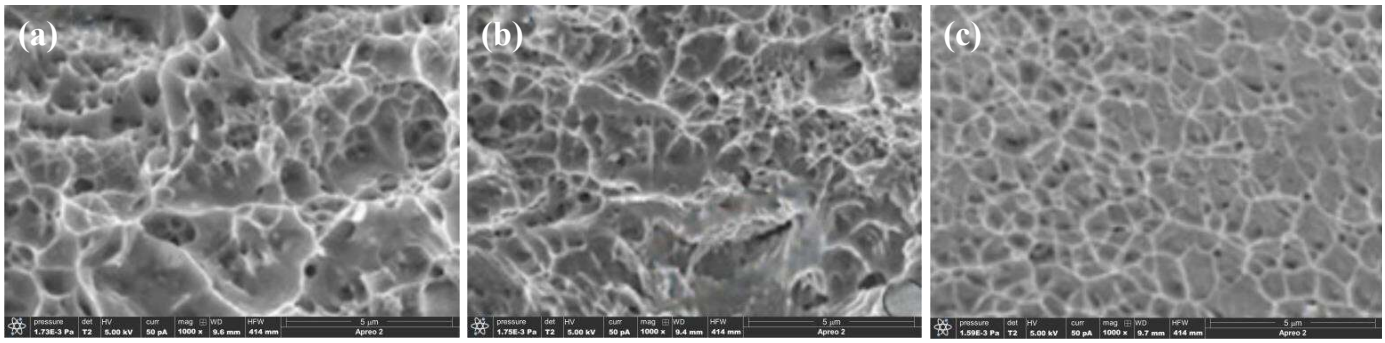

Fig. 11. Rolling image quality heat map under a variety of circumstances (a) RTR at 80%; (b) HR at 80%; (c) CR at 80%

Particle-stimulated nucleation (PSN) and dislocations create the equiaxed grains as deformation increases.

Because strain energy accumulates in the form of dislocations during cryogenic rolling, CRed specimens are known to have a greater dislocation density than RTRed specimens. Compared to CRed specimens, RTRed specimens have a larger average grain size and longer elongated grains, as seen in a microstructure study. According to OM analysis, nonrecrystallized elongated grains are present in RTRed samples, whereas recrystallized equiaxed grains are present in HRed samples, and a mixture of grains is present in CRed samples due to strain buildup along WC particles and a greater level of dislocation density. Secondary phases, represented by the black patches, can be seen laterally on the grain boundaries.

Fig. 12 depicts the grain misorientation angle distribution of the rolling sample under various handling conditions. The misorientation of grain boundaries in RTRed specimens can be identified by EBSD as either High-Angle Grain Boundaries (HAGB) (>15) or Low-Angle Grain Boundaries (LAGB). Reduced dynamic recovery at lower temperatures leads to a more concentrated distribution of LAGB in specimens with a 50% and 80% reduction in RTRed, as illustrated in lines (a) and (b) of Fig. 12. Lines (c) and (d) in the figure illustrate HRed specimens with a 50% and 80% reduction, respectively. At high temperatures, the HRed sample exhibited a higher proportion of HAGB. Nucleated recrystallized grains at the grain boundaries provide evidence of dislocation cell structure. The grain misorientation

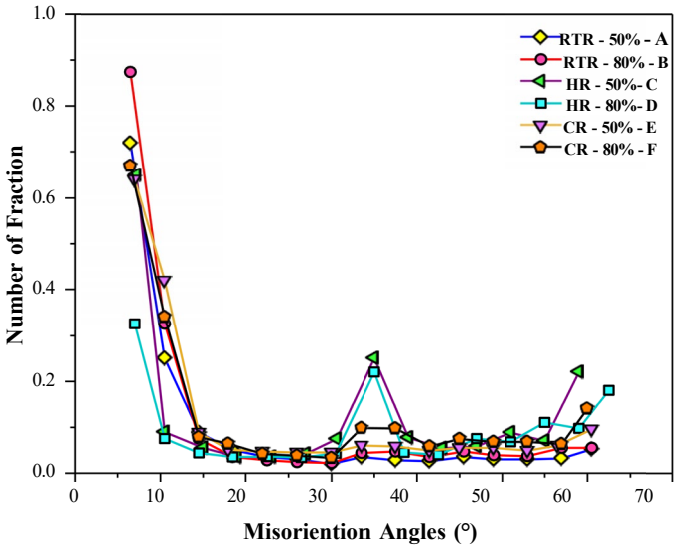

Fig. 12. Angle of disorientation relative to the proportion of Rolling in various conditions RTR

angle distribution of a 50% CRed specimen is shown in line (e) in Fig. 12, while the distribution of an 80% CRed specimen is shown in line (f) in Fig.12. A large amount of LAGB is produced all across the grain region, and dynamic recrystallisation was not seen. Dynamic recrystallisation was not seen in cryo rolled specimens of Al alloys, according to the authors [19]. This was true even after a 90% drop in rolling thickness. In contrast to RTRed samples, CRed samples have a lower LAGB proportion. The elevated dislocation density in CRed samples is due to the increased accumulation of strain energy and Tungsten Carbide particles compared to RTRed and HRed samples. A dislocation tangling zone and strong shear bands appeared, and significant deformation was observed in the CRed specimen.

Fig. 13 displays the results of an X-ray diffraction examination performed on 40 and 80% thick-reduced RTR, HR, and CR S-F specimens. XRD shows several weak peaks, indicative of secondary phases that have not been dissolved. Precipitates of $MgZn_2$, Al_2Cu, Al_7Cu_2Fe, and Al_2CuMg have been seen in RTR, HR, and CR samples. Samples reduced by 80% had somewhat brighter secondary phase peaks than those reduced by 50%. All of the samples exhibit the expected deformation peak pattern in the XRD.

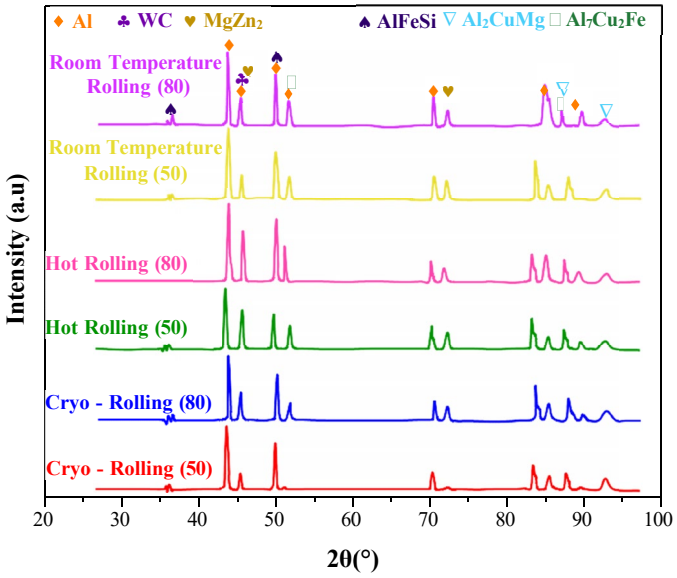

Fig. 13. XRD of various rolling of sample F with 50% and 80% reduction

The rolling method removes porosity, voids, and dendritic structure during plastic deformation, which aids in reinforcing the composite through strain hardening. Fig. 14 shows the evaluation of hardness of various rolling of sample F at 50 and 80% reduction, which has been hot rolled, room temperature rolled, and cryo rolled at 50% and 80% reduction.

Compared to sample F, hardness increases significantly at all rolling settings, as seen in Fig. 14. Maximum hardness of RTRed with 50% and 80% reduction is 170 Hv, and 158 Hv, which is 31% and 36% greater than that of sample F. Compared to sample F, the hardness of RTRed is 33% greater at 172 Hv and 39.2 percent higher at 164.5 Hv, and it is 41.8% higher at 156.5 Hv and 36 percent higher at 171.5 Hv. Fine grains, WC particles, and a greater dislocation density are all formed during rolling, contributing to the material's increased hardness. Dislocation tangles, which are the result of dislocation interaction, are formed when the density of dislocations is high.

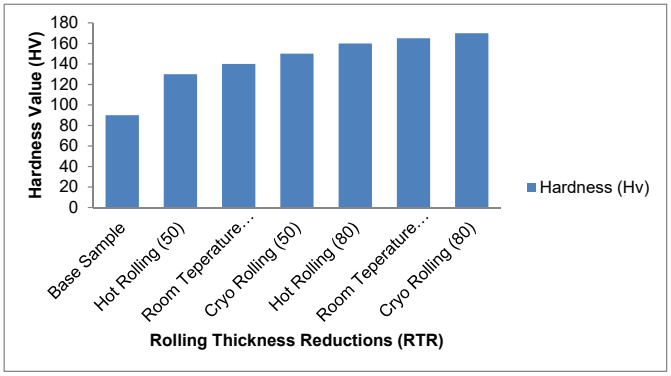

Fig. 14. Evaluation of Hardness of various rolling of sample F at 50 and 80% reduction

4. Conclusion

The mechanical and microstructural characteristics of AA6063 composite reinforced with WC particles are analyzed, focusing on strength, elongation, and hardness parameters. The findings indicate the advantageous impact of WC incorporation and cryo-rolling on the material's characteristics and the mechanisms underlying these alterations.

1. The incorporation of 1 wt.% WC enhances the mechanical properties of the AA6063 matrix, achieving a maximum ultimate tensile strength (UTS) of 235 MPa, yield strength (YS) of 210 MPa, and elongation of 2.7%. These values exceed the base alloy by 35.7%, 59.8%, and 107.6%, respectively.
2. The integration of WC particles into the semi-solid aluminium matrix promoted the transition from a dendritic to an equiaxed microstructure, hence improving the composite mechanical properties.
3. The secondary phases in the cast state ($Mg(Zn, Cu, Al)_2$ and h-(Al_2Cu)) were effectively dissolved during homogenization, as demonstrated by the X-ray diffraction (XRD) technique and microstructural investigation. The enhancement in hardness was ascribed to precipitation hardening following the ageing process.
4. The hardness of sample F composite is enhanced by an impressive 171.8% by the cryo-rolling process compared to the cryo-rolled samples, demonstrating the efficacy of the cryo-rolling procedure in augmenting material hardness.
5. The enhanced hardness of cryo-rolled materials was attributed to dislocation hardening, the inhibition of dynamic recovery, and partial grain refinement. The predominant factor among these was the reinforcing effect of temperature mismatch in rubber composites, which significantly surpassed that of grain refinement and the load transmission mechanism.

REFERENCES

[1] J.A. Muñoz, A. Komissarov, M. Avalos, R.E. Bolmaro, Heat treatment effect on an AA6063 alloy. Materials Letters **277** (2020).

[2] L. Aydi, M. Khlif, C. Bradai, S. Spigarelli, M. Cabibbo, M.E. Mehtedi, Mechanical properties and microstructure of primary and secondary AA6063 aluminum alloy after extrusion and T5 heat treatment. Materials Today: Proceedings **2** (10), 4890-4897 (2015).

[3] A. Aytaç, B. Daşçilar, M. Usta, The effect of extrusion speed on the structure and corrosion properties of aged and non-aged 6063 aluminum alloy. Materials Chemistry and Physics **130** (3), 1357-1360 (2011).

[4] O.B. Bembalge, S.K. Panigrahi, Development and strengthening mechanisms of bulk ultrafine grained AA6063/SiC composite sheets with varying reinforcement size ranging from nano to micro domain. Journal of Alloys and Compounds **766**, 355-372 (2018). DOI: https://doi.org/10.1016/j.jallcom.2018.06.306

[5] O.B. Bembalge, S.K. Panigrahi, Aging behavior of ultrafine-grained AA6063/SiC composites with varying reinforcement sizes. Materials Science and Engineering A **768**, (2019). DOI: https://doi.org/10.1016/j.msea.2019.138482

[6] O.B. Bembalge, S.K. Panigrahi, Exploring a hybrid manufacturing process to develop high performance age hardenable ultrafine grained AA6063/SiC nano-composite sheets. Journal of Manufacturing Processes **70**, 508-517 (2021). DOI: https://doi.org/10.1016/j.jmapro.2021.09.003

[7] S. Chen, Q. Liu, K. Chen, L. Huang, Effect of cryogenic rolling and aging heat treatment on microstructure and properties of Al-Zn-Mg aluminum alloy. Materials Science and Engineering of Powder Metallurgy **25** (1), 16-26 (2020).

[8] I. Dinaharan, R. Palanivel, N. Murugan, R.F. Laubscher, Predicting the wear rate of AA6082 aluminum surface composites produced by friction stir processing via artificial neural network. Multidiscipline Modeling in Materials and Structures **16** (2), 409-423 (2020). DOI: https://doi.org/10.1108/MMMS-05-2019-0102

[9] M.E. Demir, Y.H. Çelik, A. Kalkanli, The effect of rolling and aging on mechanical and tribological properties in B_4C particle reinforced Al7075 matrix composites. Journal of Materials Research and Technology **47** (12), 16187-16208 (2022).

[10] H. Granum, O.R. Myhr, T. Børvik, O.S. Hopperstad, Effect of pre-stretching on the mechanical behaviour of three artificially aged 6xxx series aluminium alloys. Materials Today Communications **27**, (2021).

[11] T. Huang, L. Shuai, A. Wakeel, G. Wu, N. Hansen, X. Huang, Strengthening mechanisms and Hall–Petch stress of ultrafine grained Al-0.3%Cu. Acta Materialia **156**, 369-378 (2018).

[12] P. Kaushik, D.K. Dwivedi, Effect of tool geometry in dissimilar Al–Steel friction stir welding. Journal of Manufacturing Processes **68**, 198-208 (2021).

[13] M.M. Krishnan, K. Marimuthu, Effect of post-weld heat treatment on dissimilar friction stir welded AA6063 and A319 aluminium alloys. International Journal of Materials Research **105** (5), 507-511 (2014). DOI: https://doi.org/10.3139/146.111054

[14] S. Krymskiy, O. Sitdikov, E. Avtokratova, M. Markushev, 2024 aluminum alloy ultrahigh-strength sheet due to two-level nano-structuring under cryorolling and heat treatment. Transactions of Nonferrous Metals Society of China **30** (1), 14-26 (2020).

[15] F. Li, T. Zhang, Y. Wu, C. Chen, K. Zhou, Microstructure, mechanical properties and crack formation of aluminum alloy 6063 produced via laser powder bed fusion. Journal of Materials Science **57** (21), 9631-9645 (2022).

[16] H. Li, W. Zhao, R. Li, Y. Liu, Progress on additive manufacturing of maraging steel. Zhongguo Jiguang **49** (14), (2022). DOI: https://doi.org/10.3788/CJL202249.1402102

[17] W. Liao, H. Qiang, W. Song, Y. Hu, C. Zhang, Effect and mechanism of room temperature rolling, cryogenic rolling and heat treatment on mechanical properties and electrical conductivity of Cu–Ni–Si alloy with continuous directional solidification. Journal of Alloys and Compounds **949**, (2023).

[18] H. Liu, S. Yu, R. Hu, X. Zhao, Y. Zhang, Effects of composite processing at room temperature and heat treatment on microstructure and mechanical properties of Ti-53Nb alloy. Rare Metal Materials and Engineering **50** (1), 43-48 (2021).

[19] T. Liu, H. Jiang, H. Sun, Y. Wang, Q. Dong, J. Zeng, F. Bian, J. Zhang, F. Chen, B. Sun, Effects of rolling deformation on precipitation behavior and mechanical properties of Al–Zn–Mg–Cu alloy. Materials Science and Engineering A **847**, (2022).

[20] O.C. Olorunyolemi, O.A. Ogunsanya, A.A. Akinwande, O.A. Balogun, M. Saravana Kumar, Enhanced mechanical behaviour and grain characteristics of aluminium matrix composites by cold rolling and reinforcement addition. Proceedings of the Institution of Mechanical Engineers, Part E: Journal of Process Mechanical Engineering **236**, (2022).

[21] C. Prakash, S. Singh, S. Sharma, H. Garg, J. Singh, H. Kumar, G. Singh, Fabrication of aluminium carbon nano tube silicon carbide particles based hybrid nano-composite by spark plasma sintering. Materials Today: Proceedings **21**, 1637-1642 (2020).

[22] H. Shen, W. Kong, C. Tang, B. Li, D. Kong, Friction and wear performances of cathodic arc ion plated TiAlSiN coating under oil lubricated condition. Journal Wuhan University of Technology Materials Science Edition **2** (6), 1301-1305 (2017).

[23] N. Singh, R.M. Belokar, R.S. Walia, Experimental investigation on microstructural and mechanical attributes of Al 7075-T6/SiC/CR/MoS_2 based green hybrid composite via advanced vacuum-sealed bottom pouring stir casting. Silicon **14** (13), 7643-7665 (2022). DOI: https://doi.org/10.1007/s12633-021-01473-x

[24] S. Souissi, H. Barhoumi, F. Elhalouani, Microstructure evolution and mechanical properties of the T6 heat treated AA6063 alloy produced by squeeze casting. Physics of Metals and Metallography **120** (8), 806-812 (2019).

[25] C.J. Villalobos-Gutiérrez, G.E. Gedler-Chacón, J.G. La Barbera-Sosa, A. Piñeiro, M.H. Staia, J. Lesage, D. Chicot, G. Mesmacque, E.S. Puchi-Cabrera, , Fatigue and corrosion fatigue behavior of an AA6063-T6 aluminum alloy coated with a WC-10Co-4Cr alloy deposited by HVOF thermal spraying. Surface and Coatings Technology **202** (18), 4572-4577 (2008).

[26] P.F. Wang, C.B. Liu, J.C. Jie, T.J. Li, An effective method to fabricate 5083 aluminum alloy with excellent corrosion resistance. Materials Science Forum **898**, 1300-1304 (2017). DOI: https://doi.org/10.4028/www.scientific.net/msf.898.1300

[27] Q. Wang, Q. Li, Y. Sun, Effects of thermomechanical treatment on microstructure and mechanical properties of β titanium alloy. Heat Treatment of Metals **43** (10), 127-132 (2018).

[28] M.E. Demir, Y.H. Çelik, E. Kilickap, A. Kalkanli, The effect of B_4C reinforcements on the microstructure, mechanical properties and wear behavior of AA7075 alloy matrix produced by squeeze casting, Proceedings of the Institution of Mechanical Engineers. Part E: Journal of Process Mechanical Engineering **237** (6), 2574-2584 (2023).

[29] X. Xu, L. Jiang, W. Lu, Y. Lu, Z. Fei, C. Cheng, Effect of rolling and subsequent heat treatment on tensile property and crystal orientation of 5052 Al alloy. Rare Metal Materials and Engineering **43** (1), 245-248 (2014).

[30] D. Xue, W. Wei, W. Shi, Y.W. Guo, S.P. Wen, X.L. Wu, H. Huang, Z.R. Nie, Effect of cold rolling on mechanical and corrosion properties of stabilised Al–Mg–Mn–Er–Zr alloy. Journal of Materials Research and Technology **15**, 6329-6339 (2021).

[31] X. Yang, Y. Jin, R. Wu, J. Wang, D. Wang, X. Ma, L. Hou, V. Serebryany, I.I. Tashlykova-Bushkevich, S.Y. Betsofen, Simultaneous improvement of strength, ductility and damping capacity of single β-phase Mg–Li–Al–Zn alloys. Metals **13** (1), (2023).

[32] M.E. Demir, M. Okumuş, Investigation of microhardness, microstructural, tribological and thermal properties of Al7075/TiO_2/kaoline hybrid metal matrix composites produced by powder metallurgy process. Advanced Engineering Materials **26** (24) (2024). DOI: https://doi.org/10.1002/adem.202401343